arXiv:1207.3203v1 [physics.atom-ph] 13 Jul 2012

Protecting atomic coherent spin states with weak measurements and feedback

T. Vanderbruggen,[1] R. Kohlhaas,[1] A. Bertoldi,[1]
S. Bernon,[1,*] A. Aspect,[1] A. Landragin,[2] and P. Bouyer[1,3]

[1]*Laboratoire Charles Fabry, Institut d'Optique,*
CNRS, Université Paris-Sud, Campus Polytechnique,
RD 128, 91127 Palaiseau cedex, France
[2]*LNE-SYRTE, Observatoire de Paris, CNRS and UPMC,*
61 avenue de l'Observatoire, F-75014 Paris, France
[3]*Laboratoire Photonique, Numérique et Nanosciences - LP2N*
Université Bordeaux - IOGS - CNRS : UMR 5298 - Bât. A30,
351 cours de la liberation, Talence, France

(Dated: July 16, 2012)

Abstract

Weak measurements provide new ways to observe and control quantum systems. Here we use weak non-destructive measurements in a feedback scheme to protect an atomic ensemble in a coherent superposition against a simple decoherence model. The feedback efficiency, defined as the ability to recover the coherence of the initial state, is studied versus the number of photons in the probe beam. This allows us to precisely characterize the trade-off between information retrieval and destructivity. The lifetime of the coherent spin state is increased by one order of magnitude when the correction cycle is iterated.

INTRODUCTION

Coherence, a crucial property of quantum systems, is reduced and eventually destroyed by interaction with the environment, which is responsible for random perturbations of the system. The stabilisation of quantum states against decoherence is therefore essential. A standard stabilisation method relies on active feedback control to monitor and counterbalance the fluctuations of a system. Nevertheless, in the quantum mechanical case, the approach cannot disregard the perturbation set by the monitoring action itself. Weak measurements [1, 2] are a powerful tool to investigate quantum systems with low disturbance, at the price of reduced information. For this property, they have been used to tomographically reconstruct atomic states [3], to measure the average single-photon trajectories in an interferometer [4] and the average single-photon wavefunction [5]. In the context of control theory, weak measurements are at the basis of active feedback protocols [6]. On the experimental side, photonic systems were recently stabilised against decoherence [7, 8], where the feedback action relied on the partial projection induced by the measurements.

Here we protect an atomic ensemble in a coherent superposition against a simple decoherence model consisting in a random rotation of the state. The feedback scheme makes use of weak non-destructive measurements with negligible projection [9] to recover the coherence of the system. The measurement relies on the dispersion induced by the atomic sample on a far off-resonance optical beam; the measurement output is used to counterbalance the noise effect through coherent microwave manipulation. We first study the case of a dichotomic rotation noise, before presenting an extension to continuous rotation angles. The proposed method can be used in atom interferometry schemes with trapped atomic samples [10].

RESULTS

Decoherence model and feedback procedure. An ensemble of N_{at} indistinguishable two-level atoms can be represented as a collective spin [11]. When the atoms are uncorrelated and in a pure state, they form a coherent spin state (CSS). CSSs have numerous applications in many-particle interferometry [12], and are used in atomic clocks, accelerometers [13] and magnetometers [14]. Three observables $\mathbf{J} = (J_x, J_y, J_z)$ are associated with a collective spin: J_z refers to the population difference between the two atomic levels, J_x and J_y to the

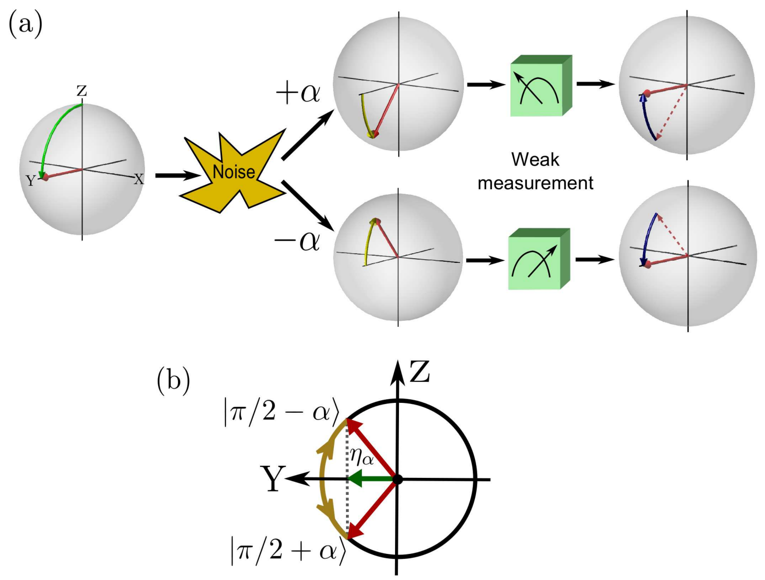

FIG. 1. **Decoherence model and feedback procedure.** (a) Evolution of the collective spin on the Bloch sphere. A $\frac{\pi}{2}$ rotation around the X axis prepares a coherent superposition. The state experiences a collective noise (a random rotation of $+\alpha$ or $-\alpha$ around the X axis), which is detected using a weak non-destructive measurement and then corrected. (b) Reduction of the coherence by the random collective rotation. The coherence of the statistical mixture generated by the noise is the length of the projection on the Y axis.

coherence between the two levels. Applying a microwave pulse we can rotate the state at will. A rotation X_θ with an angle θ around the X axis of the Bloch sphere is a coherent evolution that prepares the CSS $|\theta\rangle$ when applied on the CSS with all the atoms in the ground state.

Our experiment starts by preparing the CSS $\left|\frac{\pi}{2}\right\rangle$ (Fig. 1 (a)). We then submit the CSS to a decoherence model called random collective rotation (RCR); in the general case it consists in a rotation of random angle and axis. We first consider a dichotomic RCR where the rotation angle and axis are set, and only the rotation direction is random. We then switch to the case of a random noise angle uniformly distributed between $-\frac{\pi}{2}$ and $+\frac{\pi}{2}$ around a fix axis.

In the dichotomic case, a RCR of angle $\pm\alpha$ around the X axis of the Bloch sphere transforms the initial coherent superposition $\left|\frac{\pi}{2}\right\rangle$ in a statistical mixture of the states $\left|\frac{\pi}{2}+\alpha\right\rangle$ and $\left|\frac{\pi}{2}-\alpha\right\rangle$ with equal probability. The coherence of the atomic state is given by the length of the associated mean Bloch vector $\langle \mathbf{J} \rangle = (\langle J_x \rangle, \langle J_y \rangle, \langle J_z \rangle)$ normalized to the radius $N_{\mathrm{at}}/2$ of the Bloch sphere, where $\langle J_k \rangle = \mathrm{Tr}\,(J_k \rho)$ and ρ is the density operator of the atomic system. For a CSS the coherence is equal to unity, whereas the coherence of the mixed state generated by the RCR is $\eta_\alpha = \cos\alpha$ (see Methods and Fig. 1 (b)). As a consequence, the RCR reduces the coherence of the state.

To determine the rotation sign, we measure non-destructively the observable J_z to estimate the hemisphere where the collective spin lies after the RCR. In our feedback scheme, a controller then applies a rotation with opposite sign to that estimated for the RCR. If the detection does not resolve the atomic shot-noise then the projection of the wavefunction induced by the measurement is negligible (see Methods), and the following mixed state is achieved after the correction:

$$\rho_{\mathrm{out}} = p_s \rho\left(\frac{\pi}{2}\right) + \frac{1-p_s}{2}\left[\rho\left(\frac{\pi}{2}+2\alpha\right) + \rho\left(\frac{\pi}{2}-2\alpha\right)\right], \tag{1}$$

where $\rho(\theta) \equiv |\theta\rangle\langle\theta|$. The first term in Eq. (1) corresponds to the initial state which is properly recovered with a success probability p_s; the other two terms are related to an erroneous correction which doubles the rotation angle. The coherence of the output state ρ_{out} is $\eta_\alpha^{\mathrm{out}} = p_s + (1-p_s)\cos(2\alpha)$. If the measurement is always successful ($p_s = 1$) then $\eta_\alpha^{\mathrm{out}} = 1 > \eta_\alpha$ and the output state is pure, whereas if the measurement does not provide any information ($p_s = 1/2$) then $\eta_\alpha^{\mathrm{out}} = \eta_\alpha^2 < \eta_\alpha$ and the feedback decreases the coherence of the state. Therefore, comparing the residual coherence with or without feedback is a good criterion to evaluate the efficiency of the feedback scheme. In the specific case $\alpha = \frac{\pi}{4}$, adopted for the dichotomic RCR implementation, the estimation of the success probability is a direct measurement of the residual coherence: $\eta_{\frac{\pi}{4}}^{\mathrm{out}} = p_s$.

Experimental implementation. In our experiment, an atomic sample is trapped at the centre of an optical cavity in a butterfly configuration [15] (Fig. 2 (a)). The cavity is injected at 1550 nm for the dipole trap and at 1529 nm for the compensation of the differential light-shift on the D_2 transition (see Methods). The non-destructive detection of J_z is based on the phase-shift that the atomic sample induces on a far off-resonance optical probe [15–19]. More precisely, a frequency modulation spectroscopy technique is used to probe a cloud of ^{87}Rb atoms on the D_2 transition. The differential phase-shift between the frequency components of the probe is converted in an amplitude modulation that we detect. The system is tuned so that we directly measure J_z and thus its sign (see Methods). The population difference

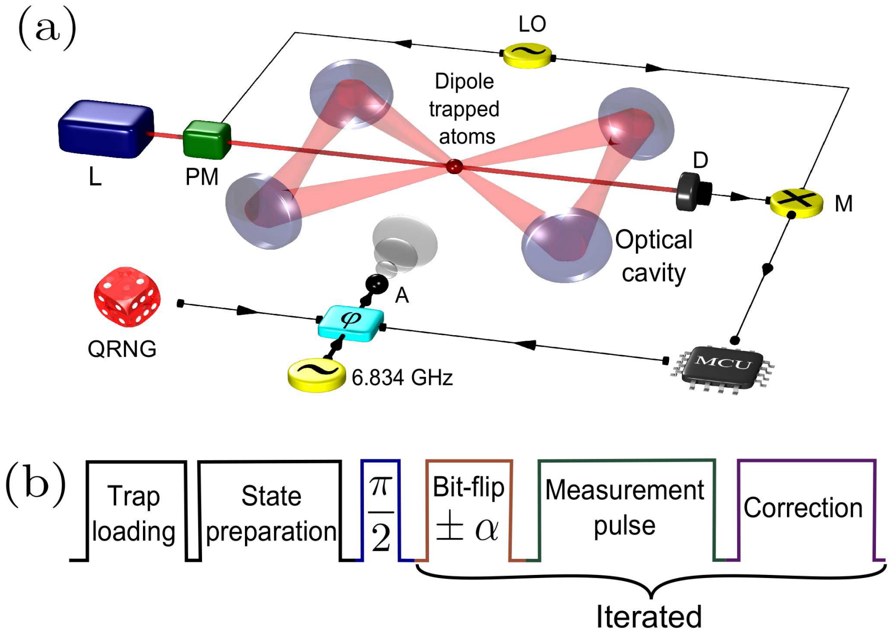

FIG. 2. **Experimental implementation.** (a) A microwave shined on the atomic sample with an antenna (A) allows us to coherently manipulate the atomic state. The detection laser at 780 nm (L) is phase modulated (PM) at 3.421 GHz with a local oscillator (LO) before passing through the atomic cloud and being detected on the photodiode (D). After demodulation in the mixer (M), the signal is digitized and sent to a microcontroller unit (MCU) that sets the phase φ of the microwave. A quantum random number generator (QRNG), connected to the phase-shifter φ, implements the RCR. (b) Experimental sequence.

between the two hyperfine levels $|0\rangle \equiv |F = 1, m_F = 0\rangle$ and $|1\rangle \equiv |F = 2, m_F = 0\rangle$ of the ground state $5^2\mathrm{S}_{1/2}$ is measured. Moreover, the inhomogeneous light-shift induced by the probe on the two levels can be a source of decoherence [15]. To remove this effect, we compensate the light-shift by precisely adjusting the power ratio between the frequency components of the probe (see Methods).

The experimental sequence (Fig. 2 (b)) begins with the preparation of the atoms in $|0\rangle$ (see Methods) and a $\frac{\pi}{2}$ microwave pulse prepares the coherent superposition between $|0\rangle$ and $|1\rangle$. The RCR is implemented as a $\frac{\pi}{4}$ microwave pulse and the rotation sign is randomly chosen by a quantum random number generator (Quantis, IDQuantique). The measurement is performed by sending a 2 μs long probe pulse. The signal is then analogically integrated to obtain its mean value over the pulse length. To implement the feedback this analog output is digitized and treated in real-time with a microcontroller. The resulting signal controls the rotation sign for the correction through the phase-shifter. The sign of the measured population difference is a straightforward indicator of the undergone rotation; as a consequence, the feedback controller applies a rotation according to the detected sign.

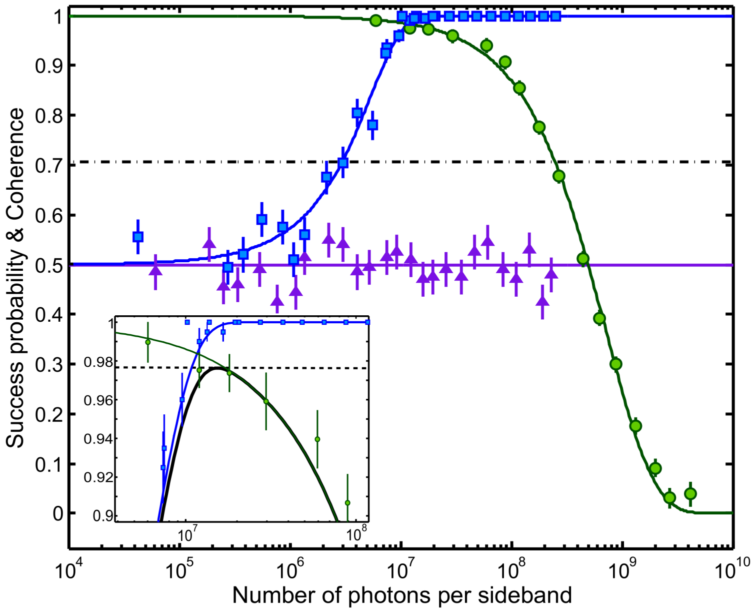

FIG. 3. **Single cycle feedback correction.** Success probability versus the number of photons per side-band in the probe pulse when the trap is loaded with 5×10^5 atoms (blue squares) and when it is empty (purple triangles). Each point has been obtained from 200 repetitions of the feedback sequence. The solid blue line is a fit of the success probability data with an error function and corresponds in this particular case ($\alpha = \frac{\pi}{4}$) to the coherence of the final state if no decoherence is induced by the probe. The green dots correspond to the measurement of the decoherence induced by the probe and the solid green line is an exponential fit of the decay of the form $\exp(-N_p/N_p^{(0)})$. The dashed black line is the coherence of the state expected for a RCR with $\eta_{\frac{\pi}{4}} = 1/\sqrt{2}$. Error bars are the ±1 standard deviation of statistical fluctuations. Inset: zoom around the optimal position. The black line is the coherence η^{out} of the output state multiplying the success probability and the spontaneous emission from the probe. The dashed line is the maximum recovered coherence.

Single feedback cycle. We first study the efficiency of the control process after a single cycle consisting in a dichotomic RCR, a weak measurement pulse and a correction rotation. For that we analyze separately the contributions of each process involved in the feedback loop: the success probability p_s and the decoherence induced by the probe. At each cycle, we store both the output of the feedback controller and that of the random number generator. We then compare these two outputs *a posteriori*, and determine the probability to produce the right correction. Fig. 3 shows the success probability as a function of the number of photons in the probe pulse (blue squares). Our data are well fitted with an error function, as expected for a Gaussian noise. We verified that no technical bias is induced by the detection beam; when the experiment is run with no atoms in the trap we observe a success probability of 1/2 (purple triangle), as expected for the random determination of a dichotomic variable. As the probe induced light shift is compensated for (see Methods), the decoherence induced by the probe is only linked to spontaneous emission processes. We then characterized this decoherence mechanism using a Ramsey interferometer (see Methods) with a probe pulse sent during the interrogation interval. The fringe contrast is a direct estimation of the residual coherence η_p. The result is shown in Fig. 3 (green dots) where we observe an exponential decay.

The coherence of the output state is finally obtained by multiplying $\eta_{\frac{\pi}{4}}^{\mathrm{out}}$ and η_p. The residual coherence of the output state reaches an optimum of 0.975 with 1.5×10^7 photons per side-band, which is the value adopted in the following. The residual coherence is larger than the coherence of the mixed state after the RCR ($\eta_{\frac{\pi}{4}} = 1/\sqrt{2}$) which proves the efficiency of the feedback scheme. This result can be improved by increasing the effective on-resonance optical depth, which allows to increase the success probability while keeping constant the amount of spontaneous emission. On the other hand, increasing the detection sensitivity to resolve the atomic shot-noise would project the atomic wavefunction [20]. This increases the uncertainty of the conjugate variable and in turns reduces the coherence of the state and thus the feedback efficiency.

Iteration of the feedback cycle.

We now study how our feedback scheme can protect a CSS over time in the presence of noise. For that we iterate 200 times the basic sequence block, consisting in the dichotomic RCR application, the detection of its effect, and the successive correction. Each cycle lasts 140 μs. Again the signs of the RCRs and the related corrections are recorded. The state at the end of each iteration is obtained by summing the angles of the RCRs and that of the corrections. It allows us to reconstruct *a posteriori*, iteration after iteration, the trajectory of the atomic state. Averaging over many realizations gives the probability for the system to

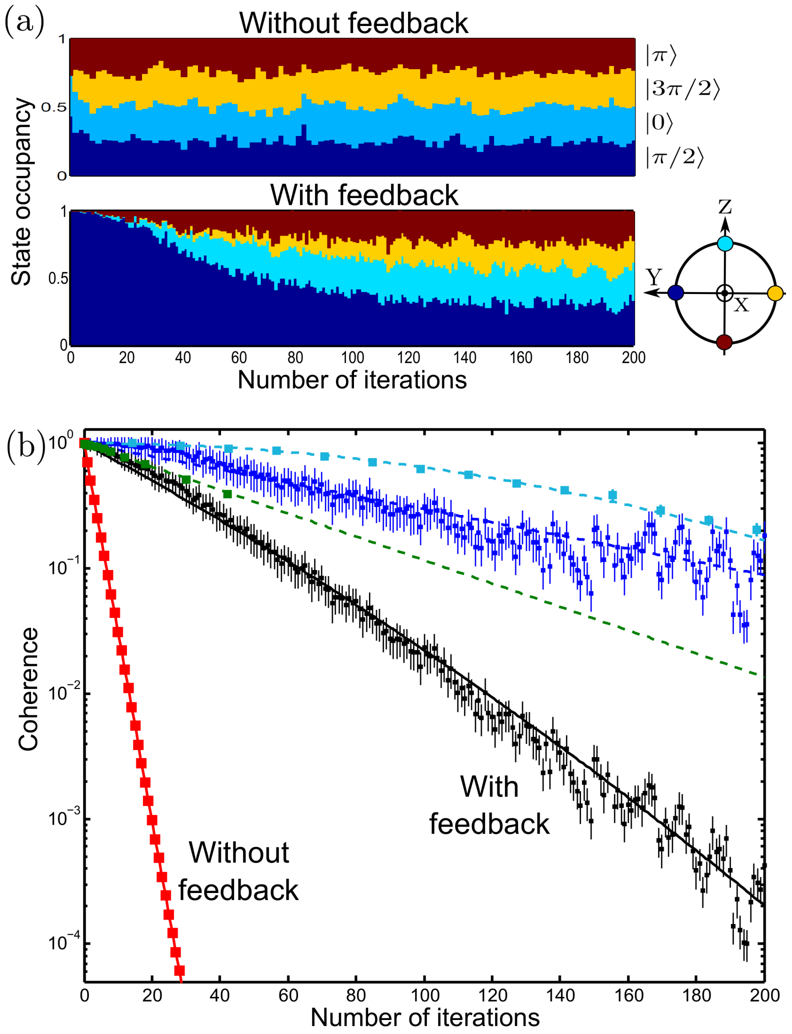

FIG. 4. **Real-time feedback sequence.** (a) State occupancy versus the number of feedback iterations for the state $|\frac{\pi}{2}\rangle$ (dark blue), $|0\rangle$ (light blue), $|\frac{3\pi}{2}\rangle$ (yellow) and $|\pi\rangle$ (red), when the feedback correction is applied (bottom) or not (top, for an even number of iterations). The state diffusion is slowed down when feedback is active. (b) Coherence evolution without (red) and with (black) feedback. The residual coherence with feedback (black) is obtained as the product of the three decoherence sources, namely the measured state occupancy (dark blue with exponential fit), the probe induced decoherence (green with exponential fit), and the light-shift of the trap beams (light blue with Gaussian fit). The error bars on the experimental points are ±1 standard deviation from statistical fluctuations and the data are obtained from 200 repetitions of the experimental sequence.

be in a given state after each iteration, as shown in Fig. 4 (a). When the noise disturbance is not corrected for, the initial state $\left|\frac{\pi}{2}\right\rangle$ experiences a random walk and diffuses rapidly. After a few iterations it is equally spread among four states : $\left\{\left|0\right\rangle, \left|\frac{\pi}{2}\right\rangle, \left|\pi\right\rangle, \left|\frac{3\pi}{2}\right\rangle\right\}$ for an even number of iterations, and $\left\{\left|\frac{\pi}{4}\right\rangle, \left|\frac{3\pi}{4}\right\rangle, \left|\frac{5\pi}{4}\right\rangle, \left|\frac{7\pi}{4}\right\rangle\right\}$ for an odd number. When the feedback correction is active, the state diffusion is slowed down by more than one order of magnitude.

The previous analysis allows us to evaluate the evolution of the coherence versus the number of iterations (see Methods). Once again, additional decoherence sources must be considered, namely: the spontaneous emission of the probe and the influence of the trapping beams. We measured both by Ramsey interferometry, and included them in the final evaluation of the coherence. The result is reported in Fig. 4 (b), and shows that the coherence with feedback is always higher than the coherence without feedback (which is $\eta_{\frac{\pi}{4}}^{N}$ after N iterations). For example, after six iterations the remaining coherence without feedback is 0.13 whereas it reaches 0.87 when a correction is applied. The feedback correction greatly improves the coherence lifetime of the system even when the experimental imperfections and limitations are taken into account.

Continuous RCR We now switch to a noise model where the random rotation angle is uniformly distributed on $[-\frac{\pi}{2}, +\frac{\pi}{2}]$. This noise generates the statistical mixture $\rho = \frac{1}{\pi}\int_{-\frac{\pi}{2}}^{+\frac{\pi}{2}} d\theta \; \left|\theta\right\rangle\left\langle\theta\right|$ which has a coherence of $2/\pi$. It is implemented using the quantum random number generator to control the length of the microwave pulse, in addition to the rotation sign. After the continuous RCR, a probe pulse with 2.8×10^{7} photons is sent to measure J_z, hence the noise angle. From the measurement result, we set both the length and the direction of the correction pulse. The feedback bandwidth is about 10 kHz and is limited by the length $\tau_\pi/2 = 75.6\ \mu s$ of the $\frac{\pi}{2}$ microwave correction pulse. A coarse feedback algorithm is implemented, which sets the correction pulse length to be proportional to the J_z measurement. The feedback has been optimized for a noise angle of $\theta = \frac{\pi}{3}$.

The feedback efficiency is characterized by measuring the length τ_N and the direction ϵ_N (+1 for a positive rotation and -1 for a negative one) for the noise pulse, and the corresponding parameters τ_C and ϵ_C for the correction pulse. The measurement is repeated 5000 times in order to compute the angular distribution $\theta_N = \pi\epsilon_N(\tau_N/\tau_\pi)$ of the CSS after the noise pulse and the angular distribution $\theta_C = \theta_N + \pi\epsilon_C(\tau_C/\tau_\pi)$ after the correction pulse, as reported Fig. 5. We find that θ_N is uniformly distributed over $[-\frac{\pi}{2}, +\frac{\pi}{2}]$ whereas θ_C is well described by a Gaussian distribution centered at zero and with a standard deviation of 200 mrad. The width of the distribution is mainly limited by the missing correction for the Z component of the Bloch vector in our setup.

The coherence of the state with and without feedback was directly measured from the contrast of Ramsey fringes (see Methods): when no feedback is applied the coherence is 0.63 ± 0.03, consistent with the expected value of $2/\pi$. When feedback is applied, the coherence increases to 0.964 ± 0.004; this is in good agreement with the Gaussian fit of Fig. 5 when the decoherence of the probe pulse is taken into account. For the correction of rotations around an arbitrary axis on the Bloch sphere one could consecutively read out J_x, J_y and J_z followed by correction rotations around two orthogonal axis of the sphere.

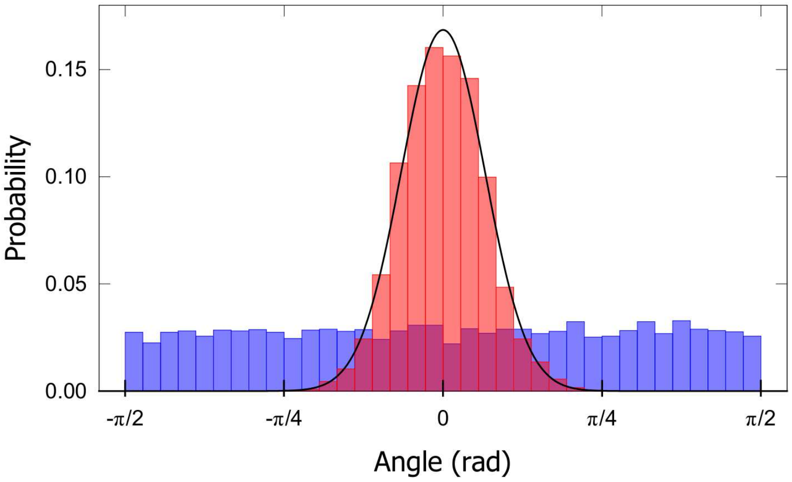

FIG. 5. **Effect of feedback for a rotation noise of random angle.** Angular probability distribution θ_N after the random rotation noise (blue) and θ_C after the correction (red), showing the reduced dispersion of the orientation. The histograms are obtained from 5000 measurements. A binning of $\frac{\pi}{36}$ is used for the histogram. The solid line is a Gaussian fit of the distribution after the correction. The fit gives a residual coherence of 0.98 for the state, which accounts only for the angular distribution and not for the destructivity of the probe pulse.

DISCUSSION

We have demonstrated that the partial information recovery provided by weak non-destructive measurements allows to implement a feedback procedure that protects an atomic CSS from the decoherence induced by RCRs. Our scheme acts as a Maxwell demon and reduces the information entropy of the system. The introduced methods can be used for the continuous interrogation and correction of the phase in atom interferometers [10]. Moreover, implementing a similar scheme in the projective measurement limit would allow a real-time control of the projection process, and thus a deterministic preparation of non-classical states [21–23] useful to improve the sensitivity of atom interferometers [16, 17, 24–28].

METHODS

Coherence of a statistical mixture of CSSs. The coordinates of the mean Bloch vector associated to the CSS $|\theta\rangle$ are:

$$\langle \mathbf{J} \rangle_\theta = \left(\langle J_x \rangle_\theta , \langle J_y \rangle_\theta , \langle J_z \rangle_\theta \right) = J \left(\sin\theta, 0, \cos\theta \right), \tag{2}$$

and the coherence of this state is $\| \langle \mathbf{J} \rangle_\theta \| / J = \sin^2\theta + \cos^2\theta = 1$.

A mixture of CSSs can be written as $\rho = \sum_k p_k \left|\theta_k\right\rangle \left\langle\theta_k\right|$, where $\sum_k p_k = 1$. From the linearity of the trace: $\langle J_l \rangle (\rho) = \mathrm{Tr}\left(J_l \rho\right) = \sum_k p_k \mathrm{Tr}\left(J_l \left|\theta_k\right\rangle \left\langle\theta_k\right|\right)$, we obtain the mean Bloch vector $\langle \mathbf{J} \rangle (\rho) = \sum_k p_k \langle \mathbf{J} \rangle_{\theta_k}$, and finally the coherence of the mixed state ρ is $\eta(\rho) = \| \langle \mathbf{J} \rangle (\rho) \| / J$, explicitly:

$$\eta(\rho) = \left[\left(\sum_k p_k \sin\theta_k\right)^2 + \left(\sum_k p_k \cos\theta_k\right)^2 \right]^{1/2} . \tag{3}$$

This relation is used to calculate the coherence of the mixture prepared by the RCR $\mathcal{E}_\alpha \left(\left| \frac{\pi}{2} \right\rangle \right)$ and the coherence of the output state ρ_{out}.

It also allows us to calculate the coherence related to the state occupancy when the feedback cycle is iterated. The probability $p_k(N)$ to be in the state $\left| \frac{\pi}{2} + k\alpha \right\rangle$ after N iterations, is related to the density matrix after N iterations through:

$$\rho_{\mathrm{out}}(N) = \sum_{k=0}^{\frac{2\pi}{\alpha}-1} p_k(N) \left| \tfrac{\pi}{2} + k\alpha \right\rangle \left\langle \tfrac{\pi}{2} + k\alpha \right| . \tag{4}$$

The contribution of the state occupancy to the coherence can thus be written as $\eta_\alpha^{\mathrm{out}}(N) = \sqrt{C_\alpha^2(N) + S_\alpha^2(N)}$, where:

$$C_\alpha(N) = \sum_{k=0}^{\frac{2\pi}{\alpha}-1} p_k(N) \cos\left(k\alpha\right), \tag{5}$$

$$S_\alpha(N) = \sum_{k=0}^{\frac{2\pi}{\alpha}-1} p_k(N) \sin\left(k\alpha\right). \tag{6}$$

Weak measurement limit. To ensure that the measurement is deep in the weak measurement limit, i.e. that the projection of the state induced by the probe pulse is negligible, the atomic shot-noise has to be much smaller than the uncertainty of the measurement. The uncertainty of the detection with 2.8×10^7 photons per probe pulse is obtained from 1000 measurements of the CSS $\left|\frac{\pi}{2}\right\rangle$. In terms of the measurement of the observable J_z that admits values in the $[-1, 1]$ range, the detection noise follows a Gaussian distribution of standard deviation $\sigma_d \sim (6.8 \pm 0.1) \times 10^{-2}$. For a cloud containing $N_{\mathrm{at}} = 5 \times 10^5$ atoms, the standard deviation of the CSS is expected to be $\sigma_{\mathrm{at}} = 1/\sqrt{N_{\mathrm{at}}} \sim 1.4 \times 10^{-3}$. The contribution of the atomic fluctuations to the measurent noise is small since $\sigma_{\mathrm{at}}/\sigma_d \sim 2\%$, as a consequence the detection is performed in the weak measurement regime.

Microwave pulses. The coherent manipulations are performed using a linearly polarized microwave field resonant with the $|F = 1, m_F = 0\rangle \rightarrow |F = 2, m_F = 0\rangle$ transition. The π pulse length is calibrated from Rabi oscillations measurements, we obtain $\tau_\pi = 151.2 \pm 0.2$ μs.

State preparation. The atoms are initially trapped in the $\left|5^2S_{1/2}, F = 1\right\rangle$ hyperfine state, and a bias field of 0.5 Gauss is applied in the direction parallel to the polarization of the non-destructive probe. The procedure to prepare the sample in the $|F = 1, m_F = 0\rangle$ state begins with a microwave π pulse followed by a light pulse on the $|F = 1\rangle \rightarrow |F' = 2\rangle$ transition to repump the residual population from the $|F = 1\rangle$ to the $|F = 2\rangle$ level. This allows to get about one third of the atoms in the $|F = 2, m_F = 0\rangle$ state. A second π pulse is applied, which populates only the $m_F = 0$ sublevel of the $|F = 1\rangle$ state. The residual atoms in the $|F = 2\rangle$ level are expelled from the trap using light tuned on the cycling transition $|F = 2\rangle \rightarrow |F' = 3\rangle$. To increase further the purity of the sample, the whole sequence is repeated twice. We characterized the prepared state using an absorption imaging technique and we measured that the cloud contains about 5×10^5 atoms at 10 μK and more than 99 % of them are polarized in the $|F = 1, m_F = 0\rangle$ state.

Measurement of the J_z observable. An optical beam is phase modulated to have 4.6 % of the total power in each side-band and passes through the atomic sample before being detected on a fast photodiode. With the two side-bands generated from the phase modulator it is possible to directly measure the population difference between the $|F = 1\rangle$ and the $|F = 2\rangle$ hyperfine levels of the ground state for an atomic ensemble: one side-band is placed close to the $|F = 1\rangle \rightarrow |F' = 2\rangle$ transition, the other one close to the $|F = 2\rangle \rightarrow |F' = 3\rangle$ transition, as depicted Fig. 6 (b). The coupling S_1 (S_2) of the first (second) side-band with the $|F=1\rangle \rightarrow |F'=2\rangle$ ($|F=2\rangle \rightarrow |F'=3\rangle$) transition, is given by:

$$S_F = \sum_{F'} \frac{\gamma \Delta_{FF'}}{\Delta^2_{FF'} + \gamma^2(1+I/I_{\rm sat})} S_{FF'}, \tag{7}$$

where γ is the half width at half maximum of the atomic transition, I the intensity of a single side-band, $I_{\rm sat}$ the saturation intensity of the transition and $S_{FF'}$ the dipolar coupling associated to the $|F\rangle \rightarrow |F'\rangle$ transition [29]. The phase-shift induced by the atomic sample on the probe is proportional to $\phi_{\rm at} \propto N_1 S_1 + N_2 S_2$, where N_1 (N_2) is the population in the $|F=1\rangle$ ($|F=2\rangle$) level. If the detunings $\Delta_{FF'}$ are adjusted so that $S_1 = -S_2$, then $\phi_{\rm at} \propto N_1 - N_2$ and the detection measures the observable J_z and eventually its sign.

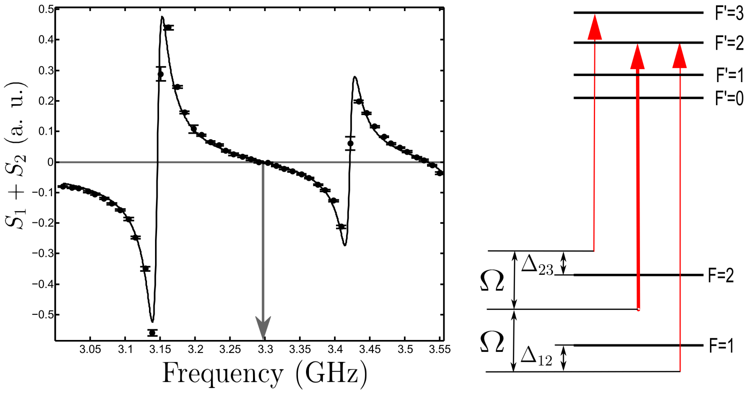

(a) (b)

FIG. 6. **Probe configuration for the measurement of J_z.** (a) Coupling of the probe versus the position of the carrier with respect to the $|F=1\rangle \rightarrow |F'=2\rangle$ transition. The points with bars are the experimental results and the solid line is the calculated coupling. (b) Hyperfine structure of ^{87}Rb D$_2$ transition and relative position of the probing beams. The thick line is the carrier whereas the thin lines are the side-bands.

To adjust the detunings $\Delta_{FF'}$, we first set a modulation frequency $\Omega = 3.4213$ GHz and prepare the atoms in a coherent superposition $\left|\frac{\pi}{2}\right\rangle$ so that $N_1 = N_2$. We measure then the demodulated signal versus the position of the carrier with respect to the $|F=1\rangle \rightarrow |F'=2\rangle$ transition. The result in Fig. 6 (a), in very good agreement with Eq. (7), was obtained with a carrier power of 153 μW and a power per side-band of 7.1 μW. The beam waist of the probe on the atomic sample is 245 μm which gives an intensity on the sample of 11.2 mW/cm^2. Since a π transition is probed, the saturation intensity is $I_{\rm sat} = 2.503$ mW/cm^2 [29]. The condition $S_1 + S_2 = 0$ is reached when the carrier is set at 3.291 GHz from the

$|F=1\rangle \rightarrow |F'=2\rangle$, in other words the detunings of the side-bands are Δ_{12} = -126.7 MHz and Δ_{23} = 148.5 MHz.

Ramsey interferometry. The fringe contrast at the output of an interferometer is a direct measurement of the ensemble coherence. We measure the coherence of the atomic CSS, by monitoring the contrast of Ramsey fringes obtained from the successive application of two $\frac{\pi}{2}$ microwave pulses separated in time. We used this method to measure the coherence loss induced by the spontaneous emission of the probe. Because the Ramsey fringes position is sensitive to light shifts, we were also able to measure the coherence loss induced by the light-shift of the trap beams, and as well accurately compensate for the light-shift induced by the probe beam.

Compensation of the probe induced light-shift. The light-shift of the probe is a severe limitation in most applications using non-destructive probing techniques, especially for interferometry since it dephases the atomic sample. Here, it would not only induce a rotation of the mean spin around the Z axis of the Bloch sphere but also spread the spins due to the spatial inhomogeneity of the Gaussian probe beam. This spread would act as a decoherence source and prevent to realize the feedback scheme if not compensated. The symmetry of the coupling of each side-band with the related transition allows to use the light-shift generated by the carrier to equally compensate that of each side-band (Fig. 7 (a)). Moreover, since the carrier and the side-bands are spatially overlapped the compensation is perfectly homogeneous. The compensation is realized by adjusting the relative power between the side-bands and the carrier. The tuning of the power ratio is precisely set using a Ramsey sequence with a probe pulse sent between the two $\frac{\pi}{2}$ pulses. Interference fringes are scanned by changing the intensity in the side-bands (Fig. 7 (b)) and the condition of maximum contrast gives the position of the zero light-shift; this is obtained with 4.6 % of the total power in each sideband.

Compensation of the differential light-shift on the D$_2$ line. Due to the $5^2P_{3/2} \rightarrow 4^2D_{5/2,3/2}$ transitions at 1529.3 nm, the trapping radiation at 1550 nm induces a differential light-shift on the D$_2$ transition [30, 31] used for the non-destructive probing. At the centre of the trap, where the radiation intensity is maximal, the frequency shift between the centre of the trap and outside is about 100 MHz which is of the same order of Δ_{12} and Δ_{23}. In such conditions, the coupling of each atom with the probe is inhomogeneous and the observable J_z is not perfectly measured. To compensate for the differential light-shift, a radiation beam at

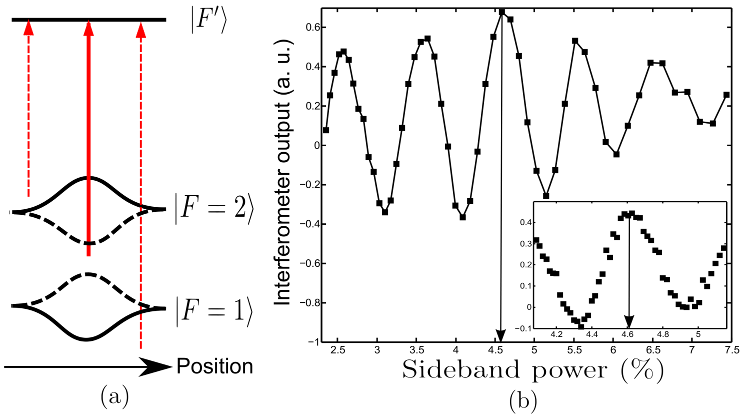

(a) (b)

FIG. 7. **Probe light-shift compensation.** (a) Light-shifts induced by the carrier (solid lines) and the side-bands (dashed lines) versus the position of an atom in the probe beam. (b) Output of a Ramsey interferometer versus the power in a single side-band in percent of the power in the carrier. A 40 μs long pulse is sent in between the two $\frac{\pi}{2}$ microwave pulse. In inset, the same measurement is performed with a 70 μs long pulse to determine more precisely the compensation ratio.

1528.7 nm, that is about 0.6 nm on the blue side of the $5^2P_{3/2} \rightarrow 4^2D_{5/2,3/2}$ transitions, was injected in the fundamental mode of the cavity [32]. By adjusting the power ratio between the 1550 nm and the 1529 nm beams, we compensate for the differential light-shift with a high spatial homogeneity thanks to the good overlap between the fundamental modes of the cavity at 1550 nm and 1529 nm. This compensation allows for a quasi-homogeneous coupling of the non-destructive probe with the atomic sample over the spatial extension of the dipole trap. The residual light-shift due to the non perfect mode overlap is about 0.7 MHz, which is not only negligible compared to Δ_{12} and Δ_{23} but also small compared to the transition linewidth ($\Gamma \sim 6$ MHz).

Acknowledgements - We thank A. Browaeys for comments. We acknowledge funding support from the Direction Générale de l'Armement (DGA), IFRAF, CNES, the European Union (EU) (project iSENSE) and ESF Euroquam. The project iSense acknowledges the financial support of the Future and Emerging Technologies (FET) programme within the Seventh Framework Programme for Research of the European Commission, under FET-Open grant number: 250072. A. B. acknowledges support from an IEF Grant PIEF-GA-2009-235375. A. A. acknowledges support from ERC QUANTATOP. P. B. acknowledges support from a chair of excellence of Région Aquitaine.

Author Contributions - T. V., R. K. and A. B. built and operated the experiment, took the data and analysed them. S. B. designed and contributed to the experimental set-up. A. L. and P. B. designed the experiment, coordinated the team and took part in the data analysis. T. V. wrote the manuscript, which was improved by R. K., A. B., S. B., A. A., A. L. and P. B.. A. L. and P. B. are the principal investigators of the project.

Author Information - Correspondence and requests for materials should be addressed to P. B. (philippe.bouyer@institutoptique.fr)

---

[*] Now at: Universität Tübingen, D-72076 Tübingen, Germany

[1] Y. Aharonov, D. Z. Albert, and L. Vaidman, "How the result of a measurement of a component of a spin-1/2 particule can turn out to be 100," Phys. Rev. Lett. **60**, 1351 (1988).

[2] N. W. M. Ritchie, J. G. Story, and R. G. Hulet, "Realization of a measurement of a 'weak value'," Phys. Rev. Lett. **66**, 1107 (1991).

[3] G. A. Smith, A. Silberfarb, I. H. Deutsch, and P. S. Jessen, "Efficient quantum-state estimation by continuous weak measurement and dynamical control," Phys. Rev. Lett. **97**, 180403 (2006).

[4] S. Kocsis, B. Braverman, S. Ravets, M. J. Stevens, R. P. Mirin, L. K. Shalm, and A. M. Steinberg, "Observing the average trajectories of single photons in a two-slit interferometer," Science **332**, 1170 (2011).

[5] J. S. Lundeen, B. Sutherland, A. Patel, C. Stewart, and C. Bamber, "Direct measurement of the quantum wavefunction," Nature (London) **474**, 188 (2011).

[6] A. M. Brańczyk, P. E. M. F. Mendonça, A. Gilchrist, A. C. Doherty, and S. D. Bartlett, "Quantum control of a single qubit," Phys. Rev. A **75**, 012329 (2007).

[7] G. G. Gillett, R. B. Dalton, B. P. Lanyon, M. P. Almeida, M. Barbieri, G. J. Pryde, J. L. O'Brien, K. J. Resch, S. D. Bartlett, and A. G. White, "Experimental feedback control of quantum systems using weak measurements," Phys. Rev. Lett. **104**, 080503 (2010).

[8] C. Sayrin, I. Dotsenko, X. Zhou, B. Peaudecerf, T. Rybarczyk, S. Gleyzes, P. Rouchon, M. Mirrahimi, H. Amini, M. Brune, J.-M. Raimond, and S. Haroche, "Real-time quantum feedback prepares and stabilizes photon number states," Nature (London) **477**, 73 (2011).

[9] S. Lloyd and J.-J. E. Slotine, "Quantum feedback with weak measurements," Phys. Rev. A **62**, 012307 (2000).

[10] N. Shiga and M. Takeuchi, "Locking the local oscillator phase to the atomic phase via weak measurement," New J. Phys. **14**, 023034 (2012).

[11] F. T. Arecchi, E. Courtens, R. Gilmore, and H. Thomas, "Atomic coherent states in quantum optics," Phys. Rev. A **6**, 2211 (1972).

[12] B. Yurke, S. L. McCall, and J. R. Klauder, "SU(2) and SU(1,1) interferometers," Phys. Rev. A **33**, 4033 (1986).

[13] A. D. Cronin, J. Schmiedmayer, and D. E. Pritchard, "Optics and interferometry with atoms and molecules," Rev. Mod. Phys. **81**, 1051 (2009).

[14] D. Budker and M. Romalis, "Optical magnetometry," Nat. Phys. **3**, 227 (2007).

[15] S. Bernon, T. Vanderbruggen, R. Kohlhaas, A. Bertoldi, A. Landragin, and P. Bouyer, "Heterodyne non-demolition measurements on cold atomic samples: towards the preparation of non-classical states for atom interferometry," New J. Phys. **13**, 065021 (2011).

[16] J. Appel, P. J. Windpassinger, D. Oblak, U. B. Hoff, N. Kjærgaard, and E. S. Polzik, "Mesoscopic atomic entanglement for precision measurements beyond the standard quantum limit," Proc. Natl. Acad. Sci. USA **106**, 10960 (2009).

[17] M. H. Schleier-Smith, I. D. Leroux, and V. Vuletić, "States of an ensemble of two-level atoms with reduced quantum uncertainty," Phys. Rev. Lett. **104**, 073604 (2010).

[18] M. Koschorreck, M. Napolitano, B. Dubost, and M. W. Mitchell, "Quantum nondemolition measurement of large-spin ensembles by dynamical decoupling," Phys. Rev. Lett. **105**, 093602 (2010).

[19] M. Kohnen, P. G. Petrov, R. A. Nyman, and E. A. Hinds, "Minimally destructive detection of magnetically trapped atoms using frequency-synthesized light," New J. Phys. **13**, 085006 (2011).

[20] T. Vanderbruggen, S. Bernon, A. Bertoldi, A. Landragin, and P. Bouyer, "Spin-squeezing and Dicke-state preparation by heterodyne measurement," Phys. Rev. A **83**, 013821 (2011).

[21] H. M. Wiseman and G. J. Milburn, "Squeezing via feedback," Phys. Rev. A **49**, 1350 (1994).

[22] L. K. Thomsen, S. Mancini, and H. M. Wiseman, "Spin squeezing via quantum feedback," Phys. Rev. A **65**, 061801(R) (2002).

[23] J. K. Stockton, J. M. Geremia, A. C. Doherty, and H. Mabuchi, "Robust quantum parameter

estimation: Coherent magnetometry with feedback," Phys. Rev. A **69**, 032109 (2004).

[24] J. Estève, C. Gross, S. Giovanazzi, and M. K. Oberthaler, "Squeezing and entanglement in a Bose-Einstein condensate," Nature (London) **455**, 1216 (2008).

[25] M. F. Riedel, P. Böhi, Y. Li, T. W. Hänsh, A. Sinatra, and P. Treutlein, "Atom-chip-based generation of entanglement for quantum metrology," Nature (London) **464**, 1170 (2010).

[26] Z. Chen, J. G. Bohnet, S. R. Sankar, J. Dai, and J. K. Thompson, "Conditional spin squeezing of a large ensemble via the vacuum Rabi splitting," Phys. Rev. Lett. **106**, 133601 (2011).

[27] B. Lücke, M. Scherer, J. Kruse, L. Pezzé, F. Deuretzbacher, P. Hyllus, O. Topic, J. Peise, W. Ertmer, J. Arlt, L. Santos, A. Smerzi, and C. Klempt, "Squeezing and entanglement in a Bose-Einstein condensate," Science **334**, 773 (2011).

[28] R. J. Sewell, M. Koschorreck, M. Napolitano, B. Dubost, N. Behbood, and M. W. Mitchell, "Spin-squeezing of a large-spin system via qnd measurement," (2011), arXiv:1111.6969.

[29] D. A. Steck, "Rubidium 87 D line data," (2001).

[30] J.-P. Brantut, J.-F. Clément, M. Robert de Saint Vincent, G. Varoquaux, R. A. Nyman, A. Aspect, T. Bourdel, and P. Bouyer, "Light-shift tomography in an optical dipole trap for neutral atoms," Phys. Rev. A **78**, 031401(R) (2008).

[31] A. Bertoldi, S. Bernon, T. Vanderbruggen, A. Landragin, and P. Bouyer, "In-situ characterization of an optical cavity using atomic light shift," Opt. Lett. **35**, 3769 (2010).

[32] R. Kohlhaas, T. Vanderbruggen, S. Bernon, A. Bertoldi, A. Landragin, and P. Bouyer, "Robust laser frequency stabilization by serrodyne modulation," Opt. Lett. **37**, 1005 (2012).